# Effect of Preburn Inhomogeneities on the Detonation Velocity in a Rotating Detonation Rocket Engine

Guillaume Vignat[a], Davy Brouzet[a], Matthias Ihme[a]
[a] Department of Mechanical Engineering, Stanford University
488 Escondido Mall, Stanford, California, United States of America

## 1  Introduction

Slow progress in the thermodynamic efficiency of deflagration-based gas turbines and rocket engines in the last few decades has sparked a renewed interest in pressure-gain combustion as a breakthrough technology to improve propulsion devices [1]. The rotating detonation rocket engine (RDRE) is a mechanically simple implementation of pressure gain combustion, requiring no moving parts and providing a near continuous thrust output. This device consists in an annular combustion chamber. Depending on the designand operating conditions, one or multiple detonation waves propagate in an azimuthal direction near the head plane of the chamber, where reactants are continuously injected so that fresh gases can replace combustion products in the short time separating the passage of two successive detonation waves. Because higher detonation velocities lead to an increased specific impulse and frequency of operation [2], detonation velocities in RDE have received considerable attention in the literature. It has been observed, both experimentally [3, 4, 5] and in simulations [6, 7, 8, 9, 10], that in configurations representative of engine geometries in which reactants are injected separately and mixed near the head plane of the chamber, the wave velocity is significantly lower than the theoretical value estimated using Chapman-Jouguet (CJ) theory [11]. For the RDRE considered in this work and over a wide range of operating conditions, Bennewitz et al. [4] report experimentally measured wave velocities in the range of $33 - 71\% \times D_{CJ}$ where $D_{CJ}$ is the theoretical CJ velocity. Several phenomena explain this lower RDRE detonation velocity. Injection systems typically used in RDREs are not conducive to thorough mixing [8, 12] and tend to be perturbed by the pressure spike associated with the passage of a detonation [8, 13]. These effects lead to imperfect combustion manifested by premature deflagrations and diffusion flames [14, 15, 8], and enlarged reaction zones [8, 15]. The presence of pockets of vitiated gases then leads to a lower pressure ratio across the detonation wave and a reduced wave velocity [15, 6]. This issue is investigated here performing a LES of the Air Force Research Laboratory (AFRL) RDRE [3, 7, 4, 8, 9]. After briefly introducing this configuration (sec. 2) and the numerical setup (sec. 3), results of the RDRE simulation are presented in sec. 4, specifically focusing on analysis of the local wave velocity and its relation to local thermodynamic variables.

## 2  The AFRL Rotating Detonation Rocket Engine

This work focuses on a RDRE that has been designed and operated for AFRL [3]. The simulations are conducted at conditions corresponding to experiments by Bennewitz et al. [4, 7]. Simulations of

this configuration were reported in previous studies [7, 8, 9]. Figure 1 shows a picture of the rig as well as a cross-section of the numerical domain used in the simulations. No simplifications were made in the geometric representation in the simulation, so that it closely mimics the experiment. This rig consists of a straight annular combustion chamber with an outer diameter of $72.6\,\mathrm{mm}$, an inner diameter of $62.6\,\mathrm{mm}$ and a length of $72.6\,\mathrm{mm}$. Reactants (oxygen and methane) are fed at the bottom of the combustion through 72 pairs of evenly spaced impinging injection port, with a total mass-flow rate of $\dot{m}_{tot} = 352\,\mathrm{g\,s^{-1}}$ and a global equivalence ratio of $\varphi = 1.16$.
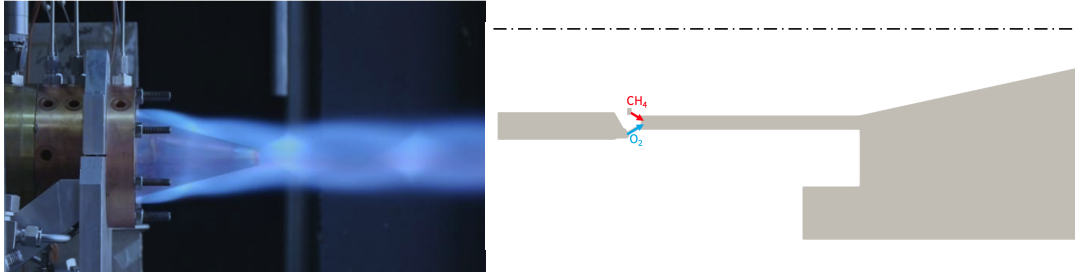


Figure 1: Left: Picture of the RDRE test rig. Reproduced from [4]; Right: Radial cut of the computational domain. A red (resp. blue) arrow indicates the fuel (resp. oxidizer) injector.

The injectors have a simple cylindrical geometry, with a diameter of $1.25\,\mathrm{mm}$ ($O_2$) and $0.79\,\mathrm{mm}$ ($CH_4$). In a given pair, the fuel and oxidizer ports are placed at the same azimuthal location and are angled towards each other by $60°$ with respect to the injection plan. Note that these injectors are not choked, but the high velocity of the reactant streams ensures the high acoustical stiffness necessary to avoid back-flow while a detonation passes over an injector pair [8]. All 72 fuel injectors are connected to a common annular methane manifold. The oxidizer injection system is set-up in a similar manner. The inlet boundary conditions for each manifold are located on their lower wall and the inlet temperature is set to $300\,\mathrm{K}$. At the end of the combustor, a $15°$ spike extends out on the centerline and the flow is exhausted to the atmosphere. In the simulation, this is represented by a cylindrical exhaust plenum with an axial co-flow of nitrogen.

## 3   Numerical Setup

An unstructured hybrid computational grid with a total of 54 million control volumes is used in the present work. Tetrahedral elements are used in the fuel and oxidizer manifolds, as well as the upper part of the combustion chamber, whilst the majority of the mesh adopts a block structured topology with hexahedral elements. Inside the injection system, the typical element size is $50\,\mu\mathrm{m}$. In the lower part of the combustion chamber, where the detonations occur, elements range in size from $50\,\mu\mathrm{m}$ to $80\,\mu\mathrm{m}$. This level of mesh refinement is on par or finer than what is reported in the literature [8, 7, 9, 14, 6]. It corresponds to approximately one third of the ZND induction length and was found to be sufficiently small to resolve the detonation cell width [16].

A fully compressible finite-volume solver [17] is used to conduct the simulations. It solves the continuity, momentum, energy and species equations with a fourth-order accurate spatial discretization scheme. A simple-balancing splitting scheme for the advection-diffusion-reaction equations is used to increase the convective timestep to a typical value of $5\,\mathrm{ns}$ [18]. The stiff reaction time-stepping is treated with a fourth-order semi-implicit Rosenbrock-Krylov scheme while the non-stiff advection/diffusion operators are solved using a third-order strong stability preserving Runge-Kutta scheme. Two shock sensors are used; the first is based on pressure and density gradients to avoid numerical instabilities in the detonation, shock and combustion regions; the second is based on species mass fraction and temperature to

avoid overshoot/undershoot of these scalars. A 2nd order essentially-non-oscillatory (ENO) reconstruction procedure is then applied on the cells where the sensors are active. Turbulent subgrid stresses (SGS) are represented using the Vreman model. A multi-species finite-rate chemistry approach is used and the chemistry is modeled with the 12 species, 38 reactions FFCMy-12 mechanism specifically designed for high pressure oxy-methane rocket engine combustion [19]. All walls in the domain are treated as no-slip and adiabatic. The inlet and outlet boundary conditions are prescribed using the locally one dimensional and inviscid (LODI) Navier-Stokes Characteristic Boundary Conditions (NSCBC) method [20] with values for the relaxation coefficients that ensure a non-reflective acoustic behavior.

To validate the computational set-up, numerical simulations of detonations propagating through a homogeneous $CH_4/O_2$ mixture with $\varphi = 1.16$ are performed in 1D and 3D configurations. These simulations are initialized with an interface representative of a CJ detonation front in premixed reactants. Several 1D simulations are performed with a grid size ranging from 100 $\mu$m to 8 mm. The 3D simulation has a mesh similar to the one used in the RDRE annular chamber and features grid sizes ranging from 30 $\mu$m to 500 $\mu$m. The detonation speeds from the 1D and 3D simulations are shown in fig. 2. For grid spacing smaller than 0.5 mm, the numerical results have a maximum absolute error of 1.5% compared to the $D_{CJ}$ theoretical value obtained from [21].
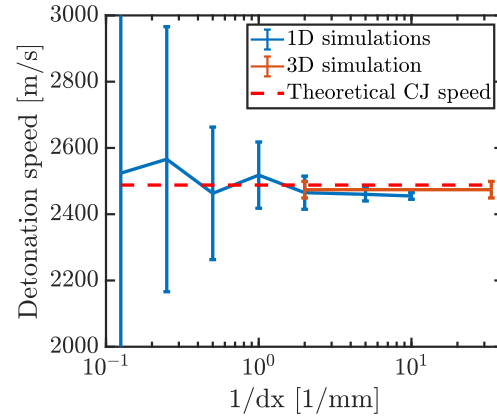


Figure 2: Comparison of detonation speed obtained in 1D and 3D simulations to the theoretical CJ velocity.

## 4   Results and discussion

In what follows, the mixture fraction is denoted as $Z$, its stoichiometric value being $Z_s = 0.8$ and the progress variable $C$ is defined as $C = Y_{CO} + Y_{CO_2} + Y_{H_2} + Y_{H_2O}$. Figure 3 shows features of the instantaneous flow field inside the RDRE. The pressure isosurface in Fig. 3a shows a high level of corrugation. The temperature field shown in the background of Fig. 3a and on a cross-sectional cut (Fig. 3b) has high levels of inhomogeneity, with a very cold center jet and localized pockets of cold gases. The temperature is naturally highly correlated with the progress variable field shown on the pressure isosurface of Fig. 3a and Fig. 3c, which shows the presence of unburnt gases in the jets formed by the injectors and in localized pockets. The detonation thus encounters a highly inhomogeneous mixture while it travels in the combustion chamber. This is further compounded by the variability of the mixture fraction in these unburnt pockets (Fig. 3d), some being fairly rich, others very lean.

The first step to examine the local detonation wave velocity is the detection of the shock itself. The shock sensor, adapted from [9], relies on two criteria. First, the regions with a pressure greater than 5 atm are identified. This condition filters out the regions potentially associated with deflagrations, which were shown to occur below this threshold value. To extract solely the detonation front, the second criterion tests if the local pressure gradient is greater than an empirical threshold value. The regions that satisfy both criteria, and which are located at a height lower than 20 mm, are then further post-processed. A method used to determine deflagration velocities [22] is then adapted to determine the local velocity of the detonation wave in the fixed frame of reference of the burner: a multipass image cross-correlation algorithm, with initial block size of 2.56 mm, final block size of 0.32 mm and 50% overlap, is applied to two solutions separated by 250 ns. The gas velocity immediately upstream of the wave front can then
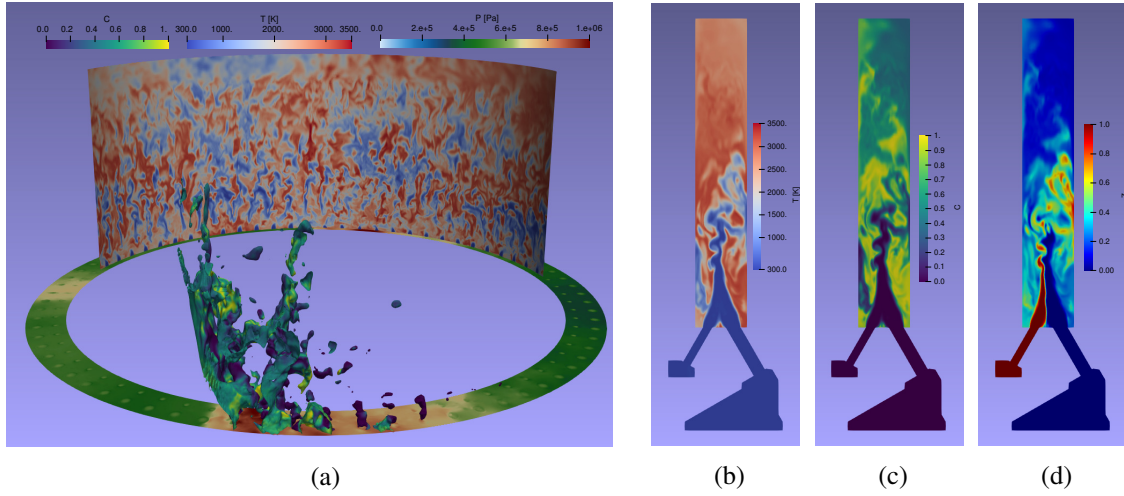
Figure 3: Instantaneous solution from the RDRE LES simulation. (a): a detonation wave is shown at the front as a pressure isosurface at $P = 850\,\text{kPa}$. The isosurface is colored by progress variable. At the bottom, a transverse slice shows the pressure field. Temperature is shown in the background. (b-d): three cross-sectional slices showing the lower $30\,\text{mm}$ of the combustion chamber and the two injection ports. This cross-section is taken far downstream of a detonation wave, along the centerline of a pair of injectors. (b): temperature (see (a) for colorscale); (c): progress variable (see (a) for colorscale); (d): mixture fraction.

be subtracted to obtain the wave velocity $D$ in the fluid reference frame. In what follows, we denote with the subscript 0 the values on the upstream side of a shock and 1 those on the downstream side. To allow comparisons with CJ theory, all reported values are taken once local equilibrium is reached, at a small distance $\delta = 2l_{in} = 0.3\,\text{mm}$ on either side of the shock, where $l_{in}$ is the ZND induction length [16].

Figure 4a-b shows scatterplots of the local value of the wave speed and Mach number at different positions on the detonation wavefront. They are shown for a sample of 12 instantaneous solutions as a function of the progress variable on the upstream side of the detonation wave and of the increase in progress variable between the upstream and downstream side of the wave. Lower wave speeds are observed in regions where unburnt gases are present. In these regions, this is associated with an increase in the progress variable across the detonation wave. In pockets of burnt gases, only shock wave propagation at higher wave velocities are observed, along with no reaction progress. In terms of Mach number, due to the higher temperature of the burnt gases, the reverse trend is observed: much higher values of $M_{det}$ tend to occur where the wave propagates as a detonation in unburnt gases. To further this analysis, we follow the approach proposed by von Neumann [23, 11] and define the variable $\lambda$ which takes value 1 when the heat release across the wave corresponds to a complete reaction and 0 when no reaction occurs. In Fig. 4c, we plot the Hugoniot curves corresponding to different values of the $\lambda$ parameter and superimpose the pressure ratios and specific volume ratios observed in the simulation. From this, one may conclude that most of the detected wavefront burns little to no fuel and the detonation is weak.

## 5   Conclusions

A large eddy simulation of the modular rotating detonation rocket engine of the Air Force Research Laboratory is conducted using a multi-species finite rate chemistry approach to model methane-oxygen pressure gain combustion. Three detonation waves are propagating azimuthally in a highly inhomogeneous gas mixture containing localized regions of unburnt and partially burnt gases. The local wave

(a)                                          (b)                                          (c)
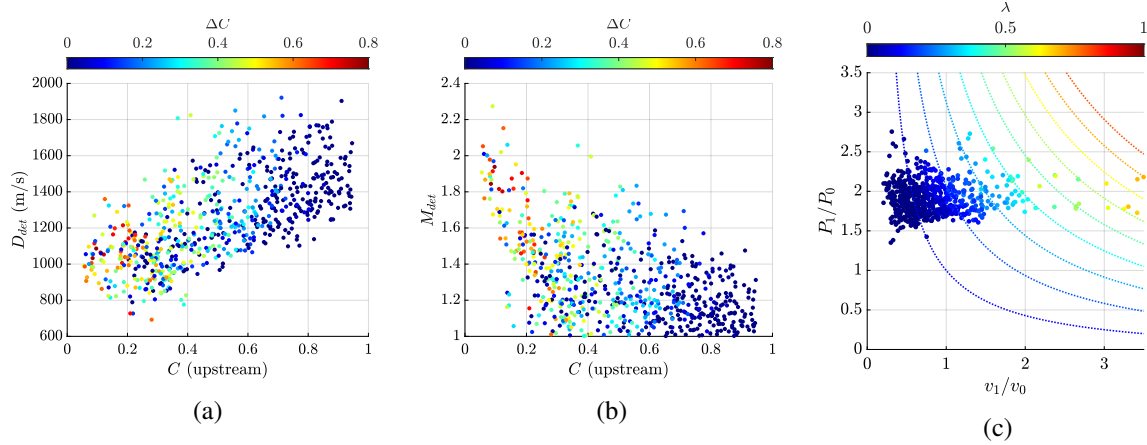
Figure 4: (a-b): Scatterplot of the local values of the detonation velocity (a) and Mach number (b) shown as a function of the progress variable upstream of the detonation wave and the change in progress variable across the wavefront. (c) Hugoniot diagram showing the pressure ratio across the wave as a function of the ratio of specific volume. The dotted line are the Hugoniot curves for a partially reacted mixture, following the approach proposed by von Neumann [23] and parametrized by $\lambda$.

velocity of the wavefront is extracted using a cross-correlation technique. We observe that this local wave velocity is highly variable: reaching typical values of 900 to $1100\,\mathrm{m\,s}^{-1}$ where the detonation front is propagating through fresh gases, it behaves as a much faster (1400 to $1500\,\mathrm{m\,s}^{-1}$) shock wave in regions of burnt gases.

## Acknowledgements

## References

[1] F. K. Lu, E. M. Braun, and J. Powers, "Rotating detonation wave propulsion: Experimental challenges, modeling, and engine concepts," *Journal of Propulsion and Power*, vol. 30, no. 5, pp. 1125–1142, 2014.

[2] J. E. Shepherd and J. Kasahara, "Analytical Models for the Thrust of a Rotating Detonation Engine," Tech. Rep., 2017.

[3] R. D. Smith and S. B. Stanley, "Experimental Investigation of Rotating Detonation Rocket Engines for Space Propulsion," *Journal of Propulsion and Power*, vol. 37, no. 3, pp. 463–473, 2021.

[4] J. W. Bennewitz, B. R. Bigler, W. A. Hargus, S. A. Danczyk, and R. D. Smith, "Characterization of detonation wave propagation in a rotating detonation rocket engine using direct high-speed imaging," in *AIAA Joint Propulsion Conference*, 2018, pp. 1–22.

[5] B. A. Rankin, D. R. Richardson, A. W. Caswell *et al.*, "Chemiluminescence imaging of an optically accessible non-premixed rotating detonation engine," *Combustion and Flame*, vol. 176, pp. 12–22, 2017.

[6] J. Fujii, Y. Kumazawa, A. Matsuo *et al.*, "Numerical investigation on detonation velocity in rotating detonation engine chamber," *Proceedings of the Combustion Institute*, vol. 36, no. 2, pp. 2665–2672, 2017.

[7] C. F. Lietz, Y. Desai, W. Hargus, and V. Sankaran, "Parametric investigation of rotating detonation rocket engines using large eddy simulations," in *AIAA Propulsion and Energy Forum and Exposition, 2019*, August 2019.

[8] S. Prakash, V. Raman, C. F. Lietz, W. A. Hargus, and S. A. Schumaker, "Numerical simulation of a methane-oxygen rotating detonation rocket engine," *Proceedings of the Combustion Institute*, vol. 38, no. 3, pp. 3777–3786, 2021.

[9] A. Batista, M. C. Ross, C. Lietz, and W. A. Hargus, "Descending modal transition dynamics in a large eddy simulation of a rotating detonation rocket engine," *Energies*, vol. 14, no. 12, pp. 1–22, 2021.

[10] S. Matsuyama, K. Iwata, Y. Nunome *et al.*, "Large-eddy simulation of rotating detonation with a non-premixed CH4/O2 injection," *AIAA Scitech 2020 Forum*, vol. 1 PartF, no. January, pp. 1–10, 2020.

[11] J. H. S. Lee, *Detonation Phenomenon.* Cambridge University Press, 2008.

[12] R. Bluemner, M. D. Bohon, C. O. Paschereit, and E. J. Gutmark, "Experimental Study of Reactant Mixing in Model Rotating Detonation Combustor Geometries," *Flow, Turbulence and Combustion*, vol. 102, no. 2, pp. 255–277, 2019.

[13] J. Burr and K. H. Yu, "Mixing in linear detonation channel with discrete injectors and side relief," in *AIAA Scitech 2019 Forum*, no. January, 2019, pp. 1–9.

[14] P. Pal, C. Xu, G. Kumar *et al.*, "Large-eddy simulation and chemical explosive mode analysis of non-ideal combustion in a non-premixed rotating detonation engine," in *AIAA Scitech 2020 Forum*, vol. 1 PartF, no. January, 2020, pp. 1–11.

[15] F. Chacon and M. Gamba, "Study of parasitic combustion in an optically accessible continuous wave rotating detonation engine," in *AIAA Scitech 2019 Forum*, no. January, 2019.

[16] S. A. Schumaker, A. M. Knisely, J. L. Hoke, and K. D. Rein, "Methane-oxygen detonation characteristics at elevated pre-detonation pressures," *Proceedings of the Combustion Institute*, vol. 38, no. 3, pp. 3623–3632, 2021.

[17] P. C. Ma, Y. Lv, and M. Ihme, "An entropy-stable hybrid scheme for simulations of transcritical real-fluid flows," *Journal of Computational Physics*, vol. 340, pp. 330–357, 2017.

[18] H. Wu, P. C. Ma, and M. Ihme, "Efficient time-stepping techniques for simulating turbulent reactive flows with stiff chemistry," *Computer Physics Communications*, vol. 243, pp. 81–96, 2019.

[19] R. Xu, K. Wang, S. Banerjee *et al.*, "A physics-based approach to modeling real-fuel combustion chemistry – II. Reaction kinetic models of jet and rocket fuels," *Combustion and Flame*, vol. 193, pp. 520–537, 2018.

[20] T. Poinsot and S. K. Lele, "Boundary conditions for direct simulations of compressible viscous flows," *Journal of Computational Physics*, vol. 101, no. 1, pp. 104–129, 1992.

[21] J. E. Shepherd, "Shock and Detonation Toolbox, https://shepherd.caltech.edu/EDL/PublicResources/sdt," 2021.

[22] S. Balusamy, A. Cessou, and B. Lecordier, "Direct measurement of local instantaneous laminar burning velocity by a new PIV algorithm," *Experiments in Fluids*, vol. 50, no. 4, pp. 1109–1121, 2011.

[23] J. von Neumann, "Theory of Detonation Waves," Tech. Rep. May 1942, 1942.